scientific reports

Check for updates

OPEN

Optimizing qubit performance through smoothing techniques

Ivan P. Malashin✉, Igor S. Masich, Vadim S. Tynchenko & Aleksei S. Borodulin

This study explores an approach to enhance the performance of qubits by leveraging signal smoothing algorithms applied to qubit chips. The primary aim is to mitigate experimental variability and enhance overall stability, tied to the improvement of the Hamiltonian spectrum. By optimizing qubit operation through smoothing techniques, data processing for subsequent stages of two-tone qubit spectroscopy data transformation is facilitated. Specifically, through the subsequent pipeline of calibration transformations for resonator frequency, qubit frequency, qubit amplitude calibrations, and refinement of qubit frequency via Ramsey oscillations, qubit state calibration can be achieved. This, in turn, improves qubit coherence time during measurement. This is because smoothing allows for a more precise determination of the Hamiltonian spectrum on two-tone spectroscopy maps, thereby enabling more accurate parameter construction.

Quantum computing, considered the next frontier in computational power, hinges on the manipulation of qubits for executing complex calculations. Although significant strides have been made in this domain, the inherent fragility of qubits and their susceptibility to environmental noise present considerable challenges. The success in the development of quantum computing based on superconducting qubits is notably exemplified by the progress achieved with transmon qubits[1]. The typical toolkit based on transmons includes a resonator with a coplanar waveguide (CPW) for dispersive readout[2] and capacitive coupling to facilitate two-qubit gates[3]. One of the key constraints in quantum computing with transmons is dielectric loss[4], which limits the coherence time of the qubit[5]. Coherence time representing the duration for which a quantum system, such as a qubit, can maintain its superposition state[6]. The presence of dielectric loss introduces decoherence mechanisms[7], limiting the stability and reliability of quantum operations performed with transmons[8].

Transmon qubit is characterized by its design incorporating a Josephson junction[9,10] shunted by a large capacitor. This design choice the anharmonicity of the qubit[11], making it less sensitive to charge noise but introduces challenges related to dielectric loss. As such, mitigating dielectric loss in transmons may extend the coherence time, ultimately enhancing the performance of quantum operation Iterative advancements in materials science and fabrication techniques have propelled a noteworthy extension in coherence times of qubits[12]. This progression, spanning from microseconds to the order of seconds[12]. By honing the composition of materials and optimizing fabrication processes[13], researchers have not only prolonged coherence times but have also significantly bolstered the dependability and efficiency of quantum computations[14]. This continuous evolution signifies a substantial leap forward in the ongoing transformation of superconducting qubit technologies. The quest to enhance the quality of information processing has ignited focused efforts to fine-tune the measurement techniques applied to qubits and resonators[15].

The resonator, serving as a tool for measuring qubits[16], shape the behavior of the quantum system. Various parameters, including the resonator's frequency range, are adjusted to optimize the measurement process and facilitate precise characterization of qubit states[17]. Two-tone spectroscopy transmission signals have proven instrumental in unraveling the energetic structure of qubits[18]. However, the complexity of the Hamiltonian, which describes the quantum system's dynamics, poses challenges. The lines indicating a fit to the spectrum of the Hamiltonian do not always yield an adequate representation[19]. The behavior of the Hamiltonian under existing parameters is not always predictable in advance.

Qubit control, as highlighted in various sources, is an aspect for achieving high precision in quantum computing and quantum information processing. The squeezed vacuum state of light, a key concept in quantum optics, reduces uncertainty in a specific quadrature compared to the coherent vacuum state. Coherent Ising machines (CIMs) based on this state can solve combinatorial optimization problems by finding the ground state[20] of the Ising model, with recent advancements in hardware solvers using optical parametric oscillators showing great promise for accelerating computational power. Existing holonomic quantum computing approaches face challenges such as decoherence errors in adiabatic HQGs and the need for additional Hilbert spaces in non-adiabatic HQGs. Li et al.[21] present a scalable, platform-independent approach using dynamical invariants to

Artificial Intelligence Technology Scientific and Education Center, Bauman Moscow State Technical University, 105005 Moscow, Russia. ✉email: ivan.p.malashin@gmail.com

realize HQGs without extra Hilbert spaces, achieving high fidelities in nuclear magnetic resonance systems, paving the way for large-scale holonomic quantum computation. Quantum systems face unwanted interactions due to environmental coupling, making efficient control crucial for quantum information processing. Zhang et al.[22] present a coupling-selective optimal control method that suppresses unwanted weak interactions and prolongs the coherence time of the desired quantum system. Applied to a 3-qubit system with one NV electron spin and two 13C nuclear spins, the method demonstrates improvements in coherence time. High-fidelity quantum coherent control impact for quantum computation and information processing. Xu et al.[23] propose a method to measure small control errors in three-level quantum systems through coherent amplification using various control techniques. By analyzing the impact of Rabi frequency errors and static detuning deviations on population transfer fidelity, it was shown that control pulse sequences can effectively amplify error detection sensitivity. This approach provides an accurate and reliable way to detect weak errors in three-level quantum systems.

The goal of this work is to employ smoothing techniques[24] to obtain a more accurate spectoscopy maps and then obtain Hamiltonian by finding extremums surfaces on these maps. By refining the fitting process, the aim is to better capture the interactions between qubits and resonators[25]. This pursuit aligns with the broader objective of advancing quantum computing technologies, ensuring the fidelity and reliability of quantum operations, and ultimately paving the way for the realization of more powerful and robust quantum processors.

Results

Two-tone spectroscopy transmission signals analysis

To obtain two-tone spectroscopy transmission signals and control the state of a qubit, a series of steps was followed (Fig. 1). Two-tone spectroscopy is a technique used to measure the qubit's frequency response while it is being driven by a probe tone and a spectroscopy tone.

The experimental setup includes a qubit, a readout resonator, and control electronics (DACs, ADCs, local oscillators, etc.). Initial calibrations are performed to determine the resonator frequency, qubit frequency. The qubit is initialized to its ground state $|0\rangle$ by waiting for a sufficiently long time or by actively resetting the qubit. The frequency of the probe tone is set to the readout resonator frequency, and the power of the probe tone is adjusted to a level that allows for readout without significantly perturbing the qubit state. The frequency of the spectroscopy tone is swept over the expected range of the qubit frequency, and its power is set to a level that drives the qubit without saturating it. The ADC is used to measure the in-phase (I) and quadrature (Q) components of the transmitted probe tone signal. The measurement is repeated multiple times, and the results are averaged to improve the signal-to-noise ratio. The magnitude and phase of the transmitted probe tone signal are plotted as a function of the spectroscopy tone frequency. Dips or peaks in the transmission spectrum that correspond to the qubit's resonance frequencies are identified.

The purpose is to highlight the diverse spectrum structures obtained under similar power levels (dBm), for both the resonator and qubit. Figure 4 illustrates examples of spectroscopy maps with the Hamiltonian spectra of qubits. The variations observed in the Hamiltonian spectra emphasize the sensitivity of the quantum system to frequency differences and offer valuable insights into the intricate dynamics of qubit-resonator interactions.

One factor affecting the quality of spectroscopy data is the variation in parameters, such as the signal power on the qubit and resonator[26]. When the resonance frequencies of the qubit and resonator are close[27], the more
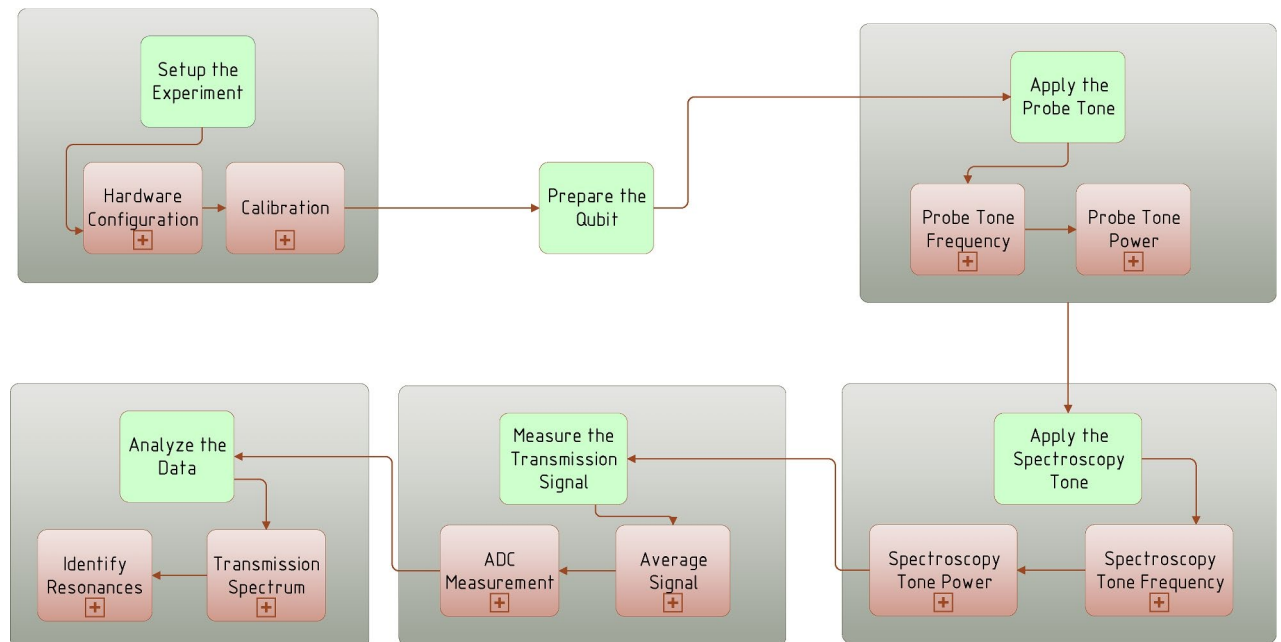

Figure 1. Steps for two-tone qubit spectroscopy.

sensitive the qubit is to the signal (i.e., it requires less power [in dBm] to be detected/observed as a line in the spectroscopy). Experimenters face the challenging task of optimizing these parameters optimal results. The spectrum of the Hamiltonian[10], represented by the yellow line in the subplot maps on Fig. 4, serves as a key reference point in this endeavor.

The second factor is the resonator frequency selected during the scanning of the qubit frequency, along with the power of the signal applied to the resonator.

Experiments involving the variation of parameters, such as signal power, often result in complex and multi-parametric maps. So, smoothing techniques become a key tool for extracting the spectrum's structure[28] and highlighting significant features under varying experimental conditions.

Smoothing

Signal smoothing techniques are explored, encompassing methods such as Lowess smoothing[29], Savitzky-Golay[30], Rolling Mean[31], Exponential Moving Average (EMA)[32], and Neural Networks including CNN[33] and RNN[34]. Special attention will be given to analyzing the impact of smoothing on Hamiltonian spectrum maps and the ability to extract signals from qubits and resonators under different experimental conditions.

The formulas for rolling mean (Eq. 1), EMA (Eq. 2), Savitzky-Golay (Eq. 3) and Lowess (Eq. 4) are shown below:

$$\mathrm{RM}_i = \frac{1}{N} \sum_{j=i-N+1}^{i} x_j \tag{1}$$

$$\mathrm{EMA}_i = \alpha \cdot x_i + (1 - \alpha) \cdot \mathrm{EMA}_{i-1} \tag{2}$$

$$\hat{y}_i = \sum_{j=-m}^{m} c_j \cdot y_{i+j} \tag{3}$$

$$\hat{y}_i = \sum_{j=1}^{n} w_{ij} \cdot y_j, \tag{4}$$

where RM_i: smoothed value using the Rolling Mean method at time i, EMA_i: smoothed value using the EMA method at time i, $\hat{y}_i$: smoothed value obtained using Savitzky-Golay or Lowess methods, x_i: current value of the time series, N: window size for Rolling Mean, α: smoothing coefficient for EMA, m: window parameter for Savitzky-Golay, c_j: coefficients of the Savitzky-Golay filter, w_{ij}: weighting coefficients for Lowess, y_i: values of the time series.

Modulation of voltage was performed under a constant voltage setting. Consequently, the focus was on studying spectrum smoothing at different frequencies while maintaining consistent voltage conditions (see Fig. 2). Observing the results, it becomes evident that Exponential Moving Average overly adapts to noise, while Rolling Mean and Savitzky-Golay introduce shifts in the spectrum's peak. Notably, Lowess emerges as the most optimal choice. Additionally, attempts were made to apply Neural Networks (NN); however, this approach did not yield satisfactory results. For voltage conditions of $- 0.05$V, 0V, and 0.05V, examples of both initial and smoothed signals using various techniques are illustrated in Fig. 2.

In addition to visual evaluation, numerical criteria was applied to select the best smoothing method. Two main criteria affecting the preservation of the global extreme after smoothing the data and reducing the noise level were considered.

The inadequacy of neural networks for signal smoothing can be attributed to their inherent complexity and capacity to model intricate patterns, which might lead to overfitting noisy data[35]. In scenarios where simplicity and adaptability are essential, traditional smoothing techniques like Lowess prove to be more effective and robust.

The obtained results will provide a better understanding of the influence of smoothing techniques on the interpretation of spectroscopic data and the optimization of experimental parameters to achieve maximum informativeness and accuracy in quantum computing research.

Figure 3 presents the density histogram of qubit magnitude values at a fixed voltage for both the original and smoothed signals. The obtained histograms were fitted using a Gaussian approximation $f(x) = A \cdot e^{-\frac{(x-\mu)^2}{2\sigma^2}}$

. This choice is justified by the Gaussian model's ability to effectively describe the distribution of values around the peak, aligning with the spectral characteristics of the qubit[36].

Subsequently, the width of the Gaussians for the original and smoothed spectra was obtained. This parameter serves as a measure of the narrowing of the value distribution in the spectrum, providing an estimate of the smoothness ratio $\mathscr{S}$ of the signal and could be described using equation 5:

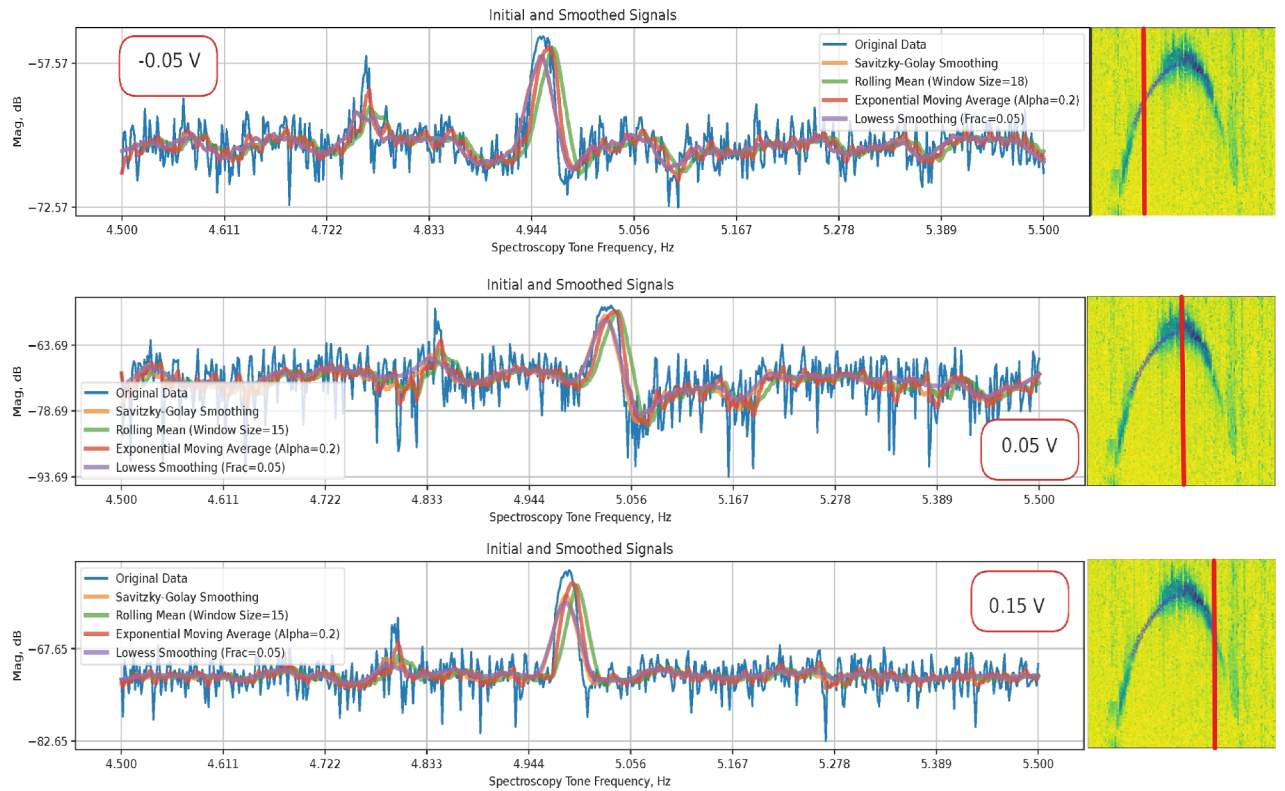$$\mathscr{S} = \frac{\sigma_{sm}}{\sigma_{in}}, \tag{5}$$

Figure 2. Three signals are presented for fixed voltage − 0.05 V (upper picture), 0.05 V (middle picture), 0.15 V (bottom picture), each obtained through smoothing techniques. Throughout the spectra, the voltage is held constant for consistent comparison. On the left side of each subplot is smoothed two-tone spectroscopy transmission signals are depicted using lowess smoothing, revealing three distinct lines. These lines correspond to different voltage conditions, with voltage held constant across the spectra.
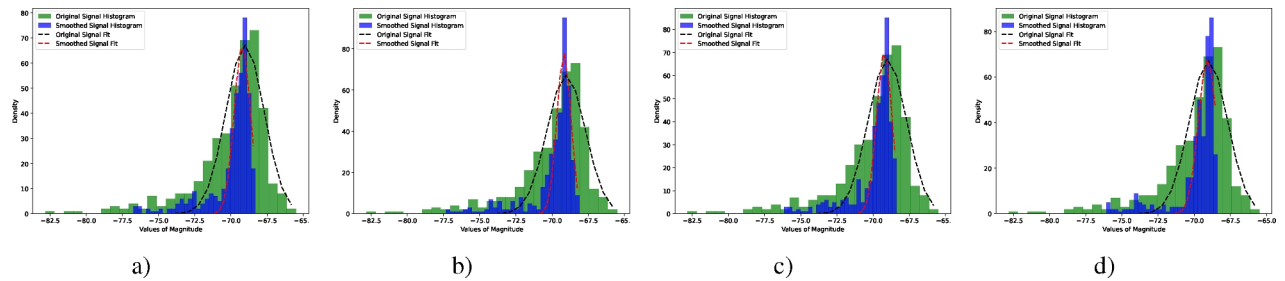

Figure 3. Density histogram of qubit magnitude values at a fixed voltage (V = − 0.05) for both the original and (**a**) Rolling Mean-, (**b**) EMA-, (**c**) Savitzky-Golay, (**d**) Lowess-smoothed signals.

where σ_{in} is the initial standard deviation of the black curve's approximated distribution of qubit magnitude values before smoothing (as shown in Fig. 3), and σ_{sm} is the standard deviation of the red curve's approximated distribution of qubit magnitude values after smoothing (as shown in Fig. 3).

The ratio of the displacement $\mathscr{R}$ of the maximum in the original and smoothed spectra was also computed and can be described using the Eq. (6):

$$\mathscr{R} = \frac{\mu_{sm}}{\mu_{in}}, \tag{6}$$

where μ_{in} is the initial mean (position of the maximum) of the black curve's approximated distribution of qubit magnitude values (as shown in Fig. 3), and μ_{sm} is the mean (position of the maximum) of the red curve's approximated distribution of qubit magnitude values after smoothing (as shown in Fig. 3).

	Rolling mean	EMA	Sav-Gol	Lowess
Narrowing	0.3683	0.3951	0.3761	0.2930
Shift	0.1062	0.0745	0.0812	0.0009

Table 1. Performance metrics for various smoothing techniques.
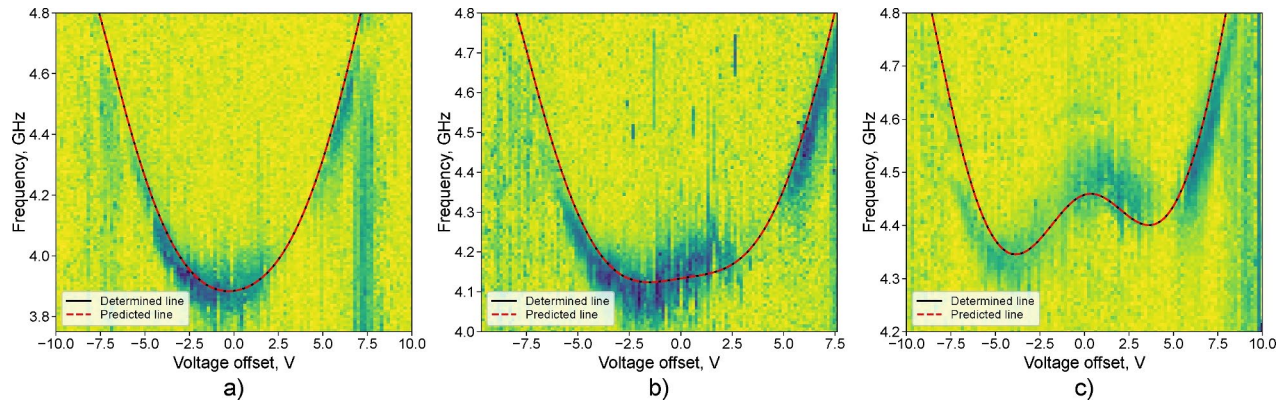

Figure 4. Detected and Predicted Hamiltonian Spectral Lines on two-tone spectroscopy maps of different qubits: The 'Determined' lines represent the spectra of the Hamiltonian determined from identified extrema, while the 'Predicted' lines are obtained through interpolation from selected extrema points on the spectroscopy maps (**a**) cubic spline, (**b**), (**c**) Lagrange interpolation.

This approach enables an assessment of how accurately the smoothing reproduces the positions of peak values. These computations were performed for all considered voltages and for each qubit.

Finally, the averaged values of width narrowing (Eq. 7) and relative displacement (Eq. 8) parameters were computed for each qubit formulas:

$$\overline{\mathscr{S}} = \frac{1}{N} \sum_{i=1}^{N} \mathscr{S}_i \tag{7}$$

$$\overline{\mathscr{R}} = \frac{1}{N} \sum_{i=1}^{N} \mathscr{R}_i, \tag{8}$$

where $\mathscr{R}_i$ is the displacement ratio for the i-th qubit, $\mathscr{S}_i$ is the width narrowing parameter for the i-th qubit, N is the total number of qubits. Thus, quality metrics (shown for all methods in Table 1) for spectrum smoothing were obtained, where larger width narrowing and smaller displacement values indicate a more effective smoothing of spectral data.

The presented table showcases metrics for qubits derived from two-tone spectroscopy data[37,38]. These values were obtained by averaging the narrowing results which were calculated by the the ratio of width of approximating Gaussians fit to the histogram of the distribution of both original and smoothed magnitude values at a constant voltage on the corresponding qubit two-tone spectroscopy map. Similarly, the "Shift" values are the average of the shifts across all qubits. Each shift was calculated by averaging the shifts for each signal at a constant voltage.

Based on Table 1, it is evident that among the various smoothing techniques, Lowess consistently demonstrates superior performance, showcasing the best results across the evaluated metric. Lowess is employed in subsequent experiments.

Interpolation of Hamiltonian spectra

During the experimental investigations, diverse two-tone spectroscopy maps were observed (see Fig. 4), unveiling the energy landscapes of qubit systems. In certain instances, the Hamiltonian spectrum manifests itself prominently like on Fig. 4a or b), discernible either in the peak or trough of magnitude profiles. However, these maps are not without challenges, as some regions exhibit isolated, noisy columns (Fig. 4c) that complicate the unequivocal identification of the Hamiltonian spectrum based solely on detected extrema.

To address this challenge, an approach in regions with noisy columns is proposed. Rather than relying solely on the values of detected extrema obtained through interpolation methods, an interpolation-based strategy utilizing the available data points is used[39]. The focus centers on contrasting spectral lines derived from

cubic splines[40] and Lagrange interpolation[41]. This method becomes particularly advantageous in regions where extrema might be obscured by noise, allowing for a more robust determination of the Hamiltonian spectrum.

This approach, at first, enhances the robustness of spectral identification in areas prone to noise[42], ensuring a more accurate representation of the underlying Hamiltonian dynamics. Secondly, the interpolation method provides a continuous and smooth representation of the spectrum, allowing for a more nuanced analysis and interpretation of the energy landscape.

Experimental results have demonstrated that the minimum number of points required for the algorithm to produce satisfactory results is 3. This determination was made through meticulous testing and experiments on diverse datasets. It should be noted that the interpolation points are chosen with approximately equal intervals, including the start, middle, and end points of the data range. This approach to point selection ensures a uniform coverage of data, thereby contributing to the stability and reliability of the Lagrangian interpolation algorithm.

The application of signal smoothing algorithms enables a more precise determination of the Hamiltonian spectrum on two-tone spectroscopy maps. By reducing noise and variability in the data, these smoothing techniques allow for a clearer and more accurate representation of the spectral features. This improved clarity facilitates the construction of more precise parameters for qubit operation, including resonator frequency, qubit frequency, and qubit amplitude calibrations. Additionally, the refinement of qubit frequency through Ramsey oscillations becomes more effective, leading to enhanced qubit state calibration. As a result, the overall stability and performance of the qubits are significantly improved, contributing to longer coherence times during measurement.

Qubit state calibration

After obtaining the Hamiltonian spectra, the resonator frequency was calibrated using data from resonator spectroscopy (f_{res}), qubit spectroscopy f_{q}, π-pulse amplitude from two-tone spectroscopy A_{q}, readout pulse amplitude A_{RO}, suggested by user qubit coherence time T_1, and by scanning the resonator frequency within a range from $f_{\text{res}} - 20\,\text{MHz}$ to $f_{\text{res}} + 20\,\text{MHz}$ with a step of 2 MHz. This process resulted in a refined resonator frequency value.

Next, the qubit frequency was calibrated using qubit spectroscopy data f_{q}, π-pulse amplitude A_{q}, readout pulse amplitude A_{RO}, the previously coarse-calibrated resonator frequency f_{res}, qubit coherence time T_1, and by scanning the qubit frequency within a range from $f_{\text{q}} - 80\,\text{MHz}$ to $f_{\text{q}} + 80\,\text{MHz}$ with a step of 4 MHz. This step yielded a refined qubit frequency value.

Finally, to calibrate the qubit amplitude, parameters included the readout pulse amplitude A_{RO}, the refined resonator frequency f_{res}, the refined qubit frequency f_{q}, qubit coherence time T_1, and scanning the π-pulse amplitude range from 0 V to 0.9 V with a step of 0.04 V. This iterative process concluded with a refined qubit amplitude value. The pipeline of proposed approach is shown on Fig. 5 as 'Calibration Techniques' section.

The refined qubit amplitude value was necessary for calibrating the qubit states $|0\rangle$ and $|1\rangle$. The parameters involved in this calibration included the readout pulse amplitude A_{RO}, precise resonator frequency calibration data f_{res}, coarse qubit frequency calibration data f_q, precise π-pulse amplitude calibration A_q, and qubit coherence time T_1.

However, often it's essential to further refine these qubit frequencies using Ramsey state data. For this purpose, the following additional data is utilized: the readout pulse amplitude A_{RO}, precise resonator frequency calibration data f_{res}, qubit frequency calibration data f_q, π-pulse amplitude calibration A_q, a time interval range from 0 μs to 1 μs with a step of 25 ns, qubit coherence time T_1, and qubit detuning f_{Ramsey}[17,43].

Refining the qubit frequency using Ramsey oscillations and adjusting the calibration curves for states $|0\rangle$ and $|1\rangle$ accordingly allows for precise alignment with the qubit frequency. Re-running the Ramsey oscillations measurement with the same detuning ensures accurate calibration to the actual detuning value f_{Ramsey} and adjusts the qubit frequency accordingly.

This iterative refinement process ensures accurate characterization and control of the qubit's quantum state dynamics, thereby enhancing the qubit's coherence time. This step in the pipeline is depicted in Fig. 5 as 'Fine-Tuning Qubit Frequency and State'.

Methods
Functions

As part of the research, Python functions were developed for processing two-tone spectroscopy data.

`create_2d_matrix` function pivots the DataFrame to create a 2D matrix representation of the data. This matrix structure organizes the data into rows and columns, with each cell containing a specific data value. By transforming the DataFrame into a matrix, the function simplifies data analysis tasks and enables the application of various analytical techniques.

`plot_heatmap` function employ to visualize the smoothed data as a heatmap. This visualization technique offers a clear and intuitive representation of the distribution of qubit magnitudes across different voltage offsets and frequencies.

`plot_heatmap_and_agr_line` is designed to determine the line of Hamiltonian spectra by finding the minimum value along the column axis of the preprocessed 2d matrix; otherwise, it identifies the line by finding the maximum value. The function plots the determined line as a dashed gray line and, if provided, the predicted line as a solid black line. It also generates a heatmap using the calculated 2D histogram, with the x-axis representing the voltage offset and the y-axis representing the frequency. Additionally, it adds a color bar to the heatmap for reference. Finally, the function displays the plot and returns an array containing the coordinates of the Hamiltonian spectra.

`smooth_matrix` function takes a matrix as input and applies a smoothing technique to reduce signal's noise and enhance the clarity of the data. It employs a specified smoothing algorithm to iteratively adjust
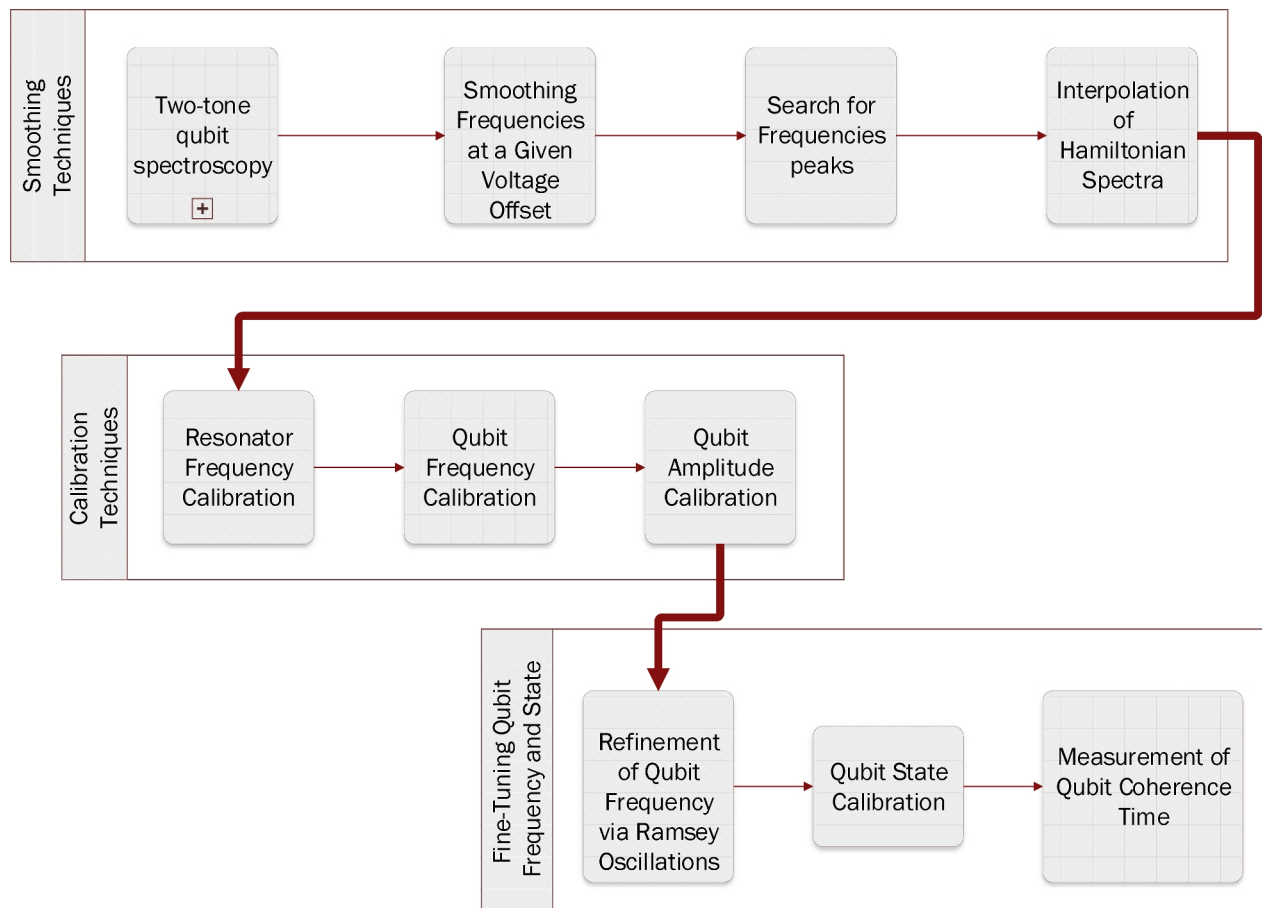
Figure 5. Experimental pipeline of the approach.

the values of each columns in the matrix, thereby minimizing fluctuations and improving overall coherence. This function is particularly useful for preprocessing data prior to visualization or analysis, ensuring that the underlying patterns and trends are more readily discernible.

`good_column` function is designed to assess the quality of columns within a dataset of two-tone spectroscopy maps, determining whether each column qualifies as good or bad based on specific criteria. It operates by analyzing the magnitudes of data points within a defined window size, evaluating their consistency to discern the reliability of the column. By iterating through the dataset, the function identifies windows where all magnitudes meet predefined conditions, such as being above or below certain thresholds depending on the presence of discretization. If the number of valid windows falls within a specified range, typically between 1 and 10, the column is classified as good; otherwise, it is considered bad. This function serves as a valuable tool for data quality evaluation, assisting in the identification of columns containing reliable information and contributing to the overall assessment of dataset integrity.

Technical validation

To validate the quality of interpolation methods, namely Lagrange approximation or spline interpolation, applied to the obtained Hamiltonian spectrum derived from extremum points in each column of every two-tone spectroscopy map, the Mean Absolute Percentage Error (MAPE) metric was utilized. MAPE is a statistical measure commonly used to assess the accuracy of forecasting models or interpolation techniques. It calculates the average absolute percentage difference between the actual and predicted values.

The mechanism for employing MAPE involves comparing the interpolated spectrum obtained from Lagrange or spline interpolation to the actual spectrum derived from extreme points. By calculating the percentage difference between the actual and interpolated values for each data point in the spectrum, MAPE provides a comprehensive evaluation of the accuracy of the interpolation method.

The advantage of utilizing MAPE lies in its ability to quantify the accuracy of the interpolation technique across the entire spectrum, capturing both large and small discrepancies between the actual and interpolated values. This holistic assessment allows researchers to identify regions where the interpolation method performs exceptionally well and areas where improvements may be necessary. Additionally, MAPE offers a standardized measure for comparing the performance of different interpolation methods, facilitating informed decision-making in selecting the most suitable technique for approximating Hamiltonian spectra in quantum computing experiments.

Data availability

The code and datasets for this research are openly accessible on Git repository: QubitSpectra. The scientific community is encouraged to explore, and build upon this work, fostering collective progress in the field.

References

1. Koch, J. et al. Charge-insensitive qubit design derived from the cooper pair box. *Phys. Rev. A* **76**, 042319 (2007).
2. Gao, Y. Y., Rol, M. A., Touzard, S. & Wang, C. Practical guide for building superconducting quantum devices. *PRX Quantum* **2**, 040202 (2021).
3. Moskalenko, I., Besedin, I., Simakov, I. & Ustinov, A. Tunable coupling scheme for implementing two-qubit gates on fluxonium qubits. *Appl. Phys. Lett.* **119** (2021).
4. Eun, S., Park, S. H., Seo, K., Choi, K. & Hahn, S. Shape optimization of superconducting transmon qubits for low surface dielectric loss. *J. Phys. D Appl. Phys.* **56**, 505306 (2023).
5. Roman, C., Ransford, A., Ip, M. & Campbell, W. C. Coherent control for qubit state readout. *New J. Phys.* **22**, 073038 (2020).
6. Zhang, Y., Deng, H., Li, Q., Song, H. & Nie, L. Optimizing quantum programs against decoherence: Delaying qubits into quantum superposition. In *2019 International Symposium on Theoretical Aspects of Software Engineering (TASE)*, 184–191 (IEEE, 2019).
7. Martinis, J. M. et al. Decoherence in josephson qubits from dielectric loss. *Phys. Rev. Lett.* **95**, 210503 (2005).
8. Berke, C., Varvelis, E., Trebst, S., Altland, A. & DiVincenzo, D. P. Transmon platform for quantum computing challenged by chaotic fluctuations. *Nat. Commun.* **13**, 2495 (2022).
9. Mamin, H. et al. Merged-element transmons: Design and qubit performance. *Phys. Rev. Appl.* **16**, 024023 (2021).
10. Nguyen, L. B. et al. High-coherence fluxonium qubit. *Phys. Rev. X* **9**, 041041 (2019).
11. Zhao, P. et al. High-contrast z z interaction using superconducting qubits with opposite-sign anharmonicity. *Phys. Rev. Lett.* **125**, 200503 (2020).
12. Wang, Y. et al. Single-qubit quantum memory exceeding ten-minute coherence time. *Nat. Photonics* **11**, 646–650 (2017).
13. Siddiqi, I. Engineering high-coherence superconducting qubits. *Nat. Rev. Mater.* **6**, 875–891 (2021).
14. Pelucchi, E. et al. The potential and global outlook of integrated photonics for quantum technologies. *Nat. Rev. Phys.* **4**, 194–208 (2022).
15. Chen, L. et al. Transmon qubit readout fidelity at the threshold for quantum error correction without a quantum-limited amplifier. *NPJ Quant. Inf.* **9**, 26 (2023).
16. Yan, F. et al. The flux qubit revisited to enhance coherence and reproducibility. *Nat. Commun.* **7**, 12964 (2016).
17. Chen, Z. *Metrology of quantum control and measurement in superconducting qubits* (University of California, Santa Barbara, 2018).
18. Wallraff, A. et al. Sideband transitions and two-tone spectroscopy of a superconducting qubit strongly coupled to an on-chip cavity. *Phys. Rev. Lett.* **99**, 050501 (2007).
19. Chirolli, L. & Burkard, G. Decoherence in solid-state qubits. *Adv. Phys.* **57**, 225–285 (2008).
20. Lu, B., Liu, L., Song, J.-Y., Wen, K. & Wang, C. Recent progress on coherent computation based on quantum squeezing. *AAPPS Bull.* **33**, 7 (2023).
21. Li, Y. et al. Dynamical-invariant-based holonomic quantum gates: Theory and experiment. *Fund. Res.* **3**, 229–236 (2023).
22. Zhang, F., Xing, J., Hu, X., Pan, X. & Long, G. Coupling-selective quantum optimal control in weak-coupling nv-13 c system. *AAPPS Bull.* **33**, 2 (2023).
23. Xu, H., Song, X.-K., Wang, D. & Ye, L. Quantum sensing of control errors in three-level systems by coherent control techniques. *Sci. China Phys. Mech. Astron.* **66**, 240314 (2023).
24. Bowman, A. W. & Azzalini, A. *Applied smoothing techniques for data analysis: the kernel approach with S-Plus illustrations*, vol. 18 (OUP Oxford, 1997).
25. Geerlings, K. L. *Improving coherence of superconducting qubits and resonators* (Yale University, 2013).
26. Karpov, D., Oelsner, G., Shevchenko, S., Greenberg, Y. S. & Il'ichev, E. Signal amplification in a qubit-resonator system. *Low Temp. Phys.* **42**, 189–195 (2016).
27. Berman, G., Chumak, A. & Tsifrinovich, V. Dynamics of a phase qubit-resonator system: Requirements for fast nondemolition readout of a phase qubit. *J. Low Temp. Phys.* **170**, 172–184 (2013).
28. Tsai, F. & Philpot, W. Derivative analysis of hyperspectral data. *Remote Sens. Environ.* **66**, 41–51 (1998).
29. Dai, Y., Wang, Y., Leng, M., Yang, X. & Zhou, Q. Lowess smoothing and random forest based gru model: A short-term photovoltaic power generation forecasting method. *Energy* **256**, 124661 (2022).
30. Press, W. H. & Teukolsky, S. A. Savitzky-golay smoothing filters. *Comput. Phys.* **4**, 669–672 (1990).
31. Randall, R. B. & Antoni, J. Rolling element bearing diagnostics-a tutorial. *Mech. Syst. Signal Process.* **25**, 485–520 (2011).
32. Klinker, F. Exponential moving average versus moving exponential average. *Math. Semesterber.* **58**, 97–107 (2011).
33. Kattenborn, T., Leitloff, J., Schiefer, F. & Hinz, S. Review on convolutional neural networks (cnn) in vegetation remote sensing. *ISPRS J. Photogramm. Remote. Sens.* **173**, 24–49 (2021).
34. Li, S., Li, W., Cook, C., Zhu, C. & Gao, Y. Independently recurrent neural network (indrnn): Building a longer and deeper rnn. In *Proceedings of the IEEE conference on computer vision and pattern recognition*, 5457–5466 (2018).
35. Yuan, W. A time-frequency smoothing neural network for speech enhancement. *Speech Commun.* **124**, 75–84 (2020).
36. Barndorff-Nielsen, O. E. Normal inverse gaussian distributions and stochastic volatility modelling. *Scand. J. Stat.* **24**, 1–13 (1997).
37. Kratochwil, B. et al. Charge qubit in a triple quantum dot with tunable coherence. *Phys. Rev. Res.* **3**, 013171 (2021).
38. Sung, Y. et al. Non-gaussian noise spectroscopy with a superconducting qubit sensor. *Nat. Commun.* **10**, 3715 (2019).
39. Zhang, C. & Qiu, F. A point-based intelligent approach to areal interpolation. *Prof. Geogr.* **63**, 262–276 (2011).
40. McKinley, S. & Levine, M. Cubic spline interpolation. *Coll. Redwoods* **45**, 1049–1060 (1998).
41. Sauer, T. & Xu, Y. On multivariate lagrange interpolation. *Math. Comput.* **64**, 1147–1170 (1995).
42. Yang, C., Soong, F. K. & Lee, T. Static and dynamic spectral features: Their noise robustness and optimal weights for asr. *IEEE Trans. Audio Speech Lang. Process.* **15**, 1087–1097 (2007).
43. Goto, H. Double-transmon coupler: Fast two-qubit gate with no residual coupling for highly detuned superconducting qubits. *Phys. Rev. Appl.* **18**, 034038 (2022).

Author contributions

I.P.M. conceived the research, conducted experiments, and wrote the manuscript. I.P.M., I.S.M., and V.S.T. contributed to the experimental design and data analysis. V.S.T. and A.S.B. provided critical insights and contributed to the manuscript preparation. All authors reviewed and approved the final version of the manuscript.

Declarations

Competing interests
The authors declare no competing interests.

Additional information
Correspondence and requests for materials should be addressed to I.P.M.

Reprints and permissions information is available at www.nature.com/reprints.

Publisher's note Springer Nature remains neutral with regard to jurisdictional claims in published maps and institutional affiliations.